Lp Norm Iterative Sparse Solution for EEG Source Localization

Peng Xu, Yin Tian, Huafu Chen, and Dezhong Yao*

***Abstract*—How to localize the neural electric activities effectively and precisely from the scalp EEG recordings is a critical issue for clinical neurology and cognitive neuroscience. In this paper, based on the spatial sparse assumption of brain activities, proposed is a novel iterative EEG source imaging algorithm, Lp norm iterative sparse solution (LPISS). In LPISS, the $l_p(p \leq 1)$ norm constraint for sparse solution is integrated into the iterative weighted minimum norm solution of the underdetermined EEG inverse problem, and it is the constraint and the iteratively renewed weight that forces the inverse problem to converge to a sparse solution effectively. The conducted simulation studies with comparison to LORETA and FOCUSS for various dipoles configurations confirmed the validation of LPISS for sparse EEG source localization. Finally, LPISS was applied to a real evoked potential collected in a study of inhibition of return (IOR), and the result was consistent with the previously suggested activated areas involved in an IOR process.**

***Index Terms*—EEG source imaging, sparse constraint, inhibition of return, inverse problem, underdetermined system, weighted minimum norm solution.**

I. Introduction

THE scalp electroencephalogram (EEG) represents electrical activity manifested by the ensemble of a great number of neurons within the brain. Estimating the location and distribution of the underlying equivalent electric generators based on the scalp EEG is the EEG inverse problem [1]. The general EEG inverse problem with an assumption of a few unknown focal activated areas is a nonlinear optimization problem. To simplify the EEG inverse problem, the complex nonlinear problem is sometimes realized by a linear approach, which is usually based on the distributed source assumption that the solution space consists of all the possible source positions [1]–[5]. Mathematically, such a linear approach can be stated as

$$Y = AX + \varepsilon \tag{1}$$

where Y is the scalp EEG recordings of $M \times 1$, M is the number of scalp electrodes. A is the lead field matrix of $M \times N$, where N is the dimension size of possible solution space. X is the source solution vector to be estimated and ε is the noise induced in the recording. For EEG inverse problem, M is usually much smaller than N, which means that the system is underdetermined, thus, the problem lacks a unique solution because there are an infinite number of possible source configurations that could explain the measured recordings Y. To obtain a physiologically feasible solution, some possible and reasonable constraints are necessary, such as the minimum norm least square solution (MNS) developed in the early effort [3]. However MNS favors the superficial source, that is to say, for a deep source, the localized source will have some bias toward the scalp surface. The currently popularly adopted one is the weighted minimum norm solution (WMNS), among which the low resolution electromagnetic tomography (LORETA) is mostly used, though its result is really blurring. Many researchers are still making great efforts to improve the spatial resolution of EEG localization methods to satisfy the requirements of neurological research [1], [5], [6].

Usually the main neural electric activities are sparsely localized, thus, a reasonable solution should not only explain the scalp recordings but also be sparsely localized [1], [4], [5]. Presently, there are three approaches to get sparse solution for EEG inverse problem. In the first approach developed in early studies, a few sparse sources were priorly supposed, and then a nonlinear optimization method was taken to solve the inverse problem. The second way was to directly solve the $l_p(p \leq 1)$ norm solution of the inverse problem, such as the l_1 norm solution [4]. In recent years, the methods based on solution space shrinking were emphasized. Starting with an initial blurring distributed source solution, such as MNS, by iteratively shrinking the solution space, the solution would converge to a relatively sparse one, such as the self-coherence enhancement algorithm (SCEA) [6] and the focal underdetermined system solver (FOCUSS) [5], [9], [10], etc. FOCUSS is a repeated WMN procedure, and it recursively adjusts the weighting matrix until most elements of the solution become nearly zero, thus, achieving a sparse solution. However, the final solution of FOCUSS largely depends on the initial source distribution usually provided by LORETA [2], [11], [12], and it is sensitive to noises and source configurations [1], [10]. Besides, during each FOCUSS iteration, a matrix inverse is needed and such an inverse calculation greatly determines the stability and validation of FOCUSS. Current efforts in improvement of FOCUSS are mainly made to improve the calculation of the matrix inverse and various techniques such as singular value decomposition (SVD) truncation and regularization technique are adopted [1], [5], [9], [10], [13].

Sparse component analysis (SCA) is a newly developed method for signal sparse decomposition, which usually takes

Manuscript received August 31, 2005; revised June 24, 2006. This work was supported by NSFC#90208003 and the 973 Project #2003CB716106, Doctor training Fund of MOE, PRC. *Asterisk indicates corresponding author.*

P. Xu, Y. Tian, and H. Chen are with the Center of Neuroinformatics, School of Life Science and Technology, University of Electronic Science and Technology of China, Chengdu 610054, China.

*D. Yao is with the Center of Neuroinformatics, School of Life Science and Technology, University of Electronic Science and Technology of China, Chengdu 610054, China (e-mail: dyao@uestc.edu.cn).

Color versions of Figs. 1–4 and 8–10 are available online at http://ieeexplore.ieee.org.

Digital Object Identifier 10.1109/TBME.2006.886640

$l_p(p \leq 1)$ norm as the constraint for signal decomposition [14]–[17]. Proposed in this paper is a novel EEG source imaging approach called Lp norm iterative sparse solution (LPISS), which integrates the $l_p(p \leq 1)$ norm constraint to an iterative procedure similar to FOCUSS. Compared to FOCUSS, LPISS is different in that the sparse solution of an intermediate auxiliary variable q is estimated by a l_p norm constrained optimization procedure, instead of by the matrix inverse, and when the algorithm converges, a sparse solution of source X is readily derived from the obtained sparse q. The method was introduced in Section II. The adopted head model and evaluation indexes were discussed in Section III. In Section IV, the algorithm was tested and compared with FOCUSS and LORETA. Finally, LPISS was applied to localize the sources of the evoked potential collected in a study of inhibition of return (IOR) in Section V. Discussions and conclusions concluded this paper in Section VI.

II. EEG Inverse Methods

A. Loreta

The weighted minimum-norm solution of EEG inverse problem can be stated as

$$\begin{cases} \min_J X^T W X \\ \text{s.t } Y = AX \end{cases} \tag{2}$$

where X is the solution vector of $N \times 1$; A is the $M \times N$ lead field matrix; Y with dimension of $M \times 1$ is the recorded scalp potentials; W is the $N \times N$ weighted matrix. The solution is

$$\hat{X} = TY, \quad \text{with} \quad T = W^{-1}A^T[AW^{-1}A^T]^+ \tag{3}$$

where $[AW^{-1}A^T]^+$ denotes the Moore-Penrose pseudo-inverse of $[AW^{-1}A^T]$. In LORETA, the weighted matrix W is defined as,

$$W = B \times \text{diag}(||a_1||, ||a_2||, \ldots\ldots, ||a_N||) \tag{4}$$

where B denotes the discrete spatial Laplacian operator; $||a_i||$ is the ith column norm of the lead field matrix A [2], [11], [12].

B. FOCUSS

FOCUSS algorithm was developed by Gorodnitsky and Rao [9], and it is an energy localized iterative procedure. To make the solution sparse and localized, a linear transform $X = Wq$ was taken, thus, formula (1) is changed to the following form:

$$\begin{cases} \min ||q|| \\ s.t: \ AWq = Y \end{cases} \tag{5}$$

FOCUSS is an iterative procedure for the underdetermined system and in its kth iteration the transform W_k is a diagonal matrix constructed by the prior iteration solution X_{k-1}, denoted by $W_k = (\text{diag}(X_{k-1}))$. The details of FOCUSS can be found in [9] and the iteration procedure can be briefly stated with the following three steps:

$$\begin{aligned} 1^0. \quad & W_k = (\text{diag}(X_{k-1})) \\ 2^0. \quad & q_k = (AW_k)^+ Y \\ 3^0. \quad & X_k = W_k q_k. \end{aligned} \tag{6}$$

The initial source distribution X_0 is usually provided by LORETA at the beginning of the iteration procedure. One FOCUSS procedure needs to repeat the above three steps for several times, when the iteration number is above the predefined maximum iteration number or the difference between the neighbouring iterations is smaller than the termination tolerance error, the iteration will be terminated and a sparse and energy localized solution will be achieved.

C. l_p Norm Sparse Solution

The $l_p(p \leq 1)$ norm is a quantitive index to measure the sparsity of a signal [14]–[17]. A $l_p(p \leq 1)$ norm solution is sparser and more localized than MNS [1], [4]. If the $l_p(p \leq 1)$ norm of the solution is taken as a constraint, we have a Lagrange multiplier expression of the inverse problem (1)

$$\arg\min ||Y - AX||_2 + \lambda ||X||_p \tag{7}$$

where λ is a regularization parameter [18]. For EEG source imaging, l_1 norm solution is usually adopted [1], [4]. Many optimization algorithms can be used to solve the above optimization problem and in this paper BFGS is taken for the optimization [19].

D. Lp Norm Iterative Sparse Solution (LPISS)

1) Derivation of LPISS From $l_p(p \leq 1)$ Norm Solution and FOCUSS: Both the above $l_p(p \leq 1)$ norm solution and FOCUSS aim at a sparse solution, and if they are integrated properly, a better sparse solution is possible.

As shown in step 2 of FOCUSS, it is necessary to estimate the inverse of the matrix AW to evaluate q, and such calculation is very sensitive to noise because the lead field matrix A is seriously ill-posed in an EEG inverse problem [1]. The solution may be unstable especially when the SVD of the ill-posed matrix AW is not correctly truncated or the regularization parameter is not properly selected. Current effort in improvement of FOCUSS is mainly focused on the matrix inverse or the solution space compression [1], [5], [9], [10], [13].

According to steps 2 and 3 of FOCUSS, the *ith* element of the kth iteration solution X_k, $X_k(i)$, can be formulized as

$$X_k(i) = \sum_j W_k(i,j) q_k(j) \quad i = 1, 2 \ldots N; \quad j = 1, 2 \ldots N. \tag{8}$$

Because W_k is a diagonal matrix constructed from the prior iterative solution X_{k-1}, the above formula (8) can be simplified to

$$X_k(i) = W_k(i,i)q_k(i) \quad i = 1, 2 \ldots N. \tag{9}$$

From (9), it is easy to see that if q_k is sparse, X_k is sparse too. This fact means that if we get a sparse solution of q, we actually get a sparse solution of X. Thus, in order to achieve a sparsely localized solution, we may combine the linear transform $X = Wq$ of FOCUSS into (1), and directly estimate the sparse solution of the intermediate auxiliary variable q_k by the $l_p(p \leq 1)$ norm constraint as

$$\arg\min ||Y - AW_k q_k||_2 + \lambda ||q_k||_p \tag{10}$$

where λ is a regularization parameter and W_k is a weight matrix supposed to change in the way of FOCUSS. Thus, by evaluation of the sparse expression of q_k, a sparse solution of X_k will be easily achieved at the same time. Furthermore, during the sparse solution evaluation for q_k, the noise effect will be greatly suppressed by the $l_p(p \leq 1)$ norm constrained object function as confirmed in previous studies [17]. The optimum λ can be determined by parameter regularizing criteria [18]. Usually the higher the noise power is, the larger the λ is. Chen proposed in [17] that λ could be simply determined as: $\lambda = \sigma\sqrt{2\log N}$, where σ is the standard deviation of noise and N is the size of the solution space. Specially, when $\lambda = 0$, LPISS reduces to the original FOCUSS algorithm, and when $W_k = I$, LPISS reduces to the original $l_p(p \leq 1)$ norm solution, too.

2) Procedure of LPISS: The iterative procedure of LPISS is as follows:

a) Initialization. Set $k = 1$, iteration termination error ε and the maximum iteration number $T_{\max}$, initialize source distribution X_{k-1} with LORETA solution.
b) Update the diagonal weight matrix: $W_k = (\mathrm{diag}(X_{k-1}))$.
c) Using BFGS optimization method to estimate the sparse solution of the auxiliary variable q_k : $\arg\min ||Y - AW_k q_k||_2 + \lambda ||q_k||_p$.
d) Update source distribution: $X_k = W_k q_k$.
e) Judge termination condition. Comparing the difference between the prior and the last source distribution, if $||X_k - X_{k-1}|| \leq \varepsilon$ or $k \geq T_{\max}$, terminate the iteration and X_k is the final source distribution; else $k = k + 1$, and jump to step 2 and go on.

Our method is a $l_p(p \leq 1)$ norm constrained iterative sparse solution (LPISS), and it is an integration of the repeated WMNS (FOCUSS) and the $l_p(p \leq 1)$ norm sparse solution, where the intermediate auxiliary variable q in FOCUSS was introduced into the $l_p(p \leq 1)$ norm constrained cost function for a sparse solution as (10), and the $l_p(p \leq 1)$ norm sparse solution obtained by BFGS optimization was utilized instead of the MNS of q in FOCUSS. In our practice, l_1 norm is taken as the constraint and the optimization problem is solved with BFGS [19].

III. Head Model and Evaluation Indexes

A. Head Model

A 3-shell realistic head model is used for EEG source localization, whose conductivities for cortex, skull and scalp are $1.0\ \Omega^{-1}\mathrm{m}^{-1}, 1/80\ \Omega^{-1}\mathrm{m}^{-1}$ and $1.0\ \Omega^{-1}\mathrm{m}^{-1}$, respectively. The solution space is restricted to cortical gray matter, hippocampus and other possible source activity areas, consisting of 910 cubic mesh voxels with 10 mm inter-distance. The lead field matrix A is calculated with dipole model by boundary element method (BEM) [20] for a 128 electrode system and it is a matrix with dimension of 128×2730, where $2730 = 910 \times 3$. The origin of the coordinate system is defined as the midpoint between the left and right preauriculars, and the directed line from the origin through the nasion defines the $+X$-axis, the $+Y$-axis is the directed line from the origin through the left preauricular. Finally, the $+Z$-axis is the line from the origin toward the top of the head (through electrode Cz).

B. Evaluation Indexes

Localization ability is a primary concern of inverse problem and the resolution matrix, $R = A^+A$, is a popular index for evaluation of it [1], but for LPISS, no inverse matrix A^+ is evaluated (the auxiliary variable q is estimated with BFGS optimization procedure), so we are not able to give the resolution matrix of LPISS. In this paper, we take the following three evaluation indexes. One is the localization error [1], [5], $E_{\mathrm{localization}}$, which is the distance between the simulated source and the estimated source of maximum power within a sphere neighbour of the simulated source; the second is the source energy error [5], E_{energy}, which is used to measure the source energy recovery ability. E_{energy} is defined as follows, $E_{\mathrm{energy}} = (||J_{\mathrm{simu}} - J_{\max}||/||J_{\mathrm{simu}}||)$, where J_{simu} is the moment of simulated source, $J_{\max}$ is the moment of estimated source with maximum power within a sphere neighbor of the corresponding simulated source. The third is the normalized burring index (NBI) in region of interest (ROI) to measure the spatial resolution ability [12], which is defined as shown in the equation at the bottom of the page, where the subscript i refers to a grid point of the discrete solution space in the 3-D model, for the assumed dipole distribution, it is selected as the actual position of the simulated dipole. For the reconstructed distributions, it is selected as the point with maximum power within a sphere neighbor of the corresponding simulated

$$\mathrm{NBI}_i = \sqrt{\sum_k ||r_k - r_i||^2 J^2(k) / \sum_k J^2(k)} \Bigg/ \sqrt{\sum_k ||r_k - r_i||^2 / \sum_k 1}$$

source. The subscript k refers to the neighboring points within the spherical ROI surrounding the point i. The r_k and r_i are the spatial location vectors corresponding to the grid points k and i, respectively. NBI can exhibit the distribution of sources in ROI. Generally, the smoother the sources spread in ROI, the closer to 1 the NBI is; otherwise, if the sources are sharply distributed, NBI is close to 0. Obviously, for far isolated sources, a small NBI is expected. An excellent localization algorithm should be of low $E_{\text{localization}}, E_{\text{energy}}$, and a NBI similar to the actual NBI.

In this paper, our simulations were conducted under different noise-to-signal-ratio (NSR), where NSR is defined as the ratio between the power of noise and that of signal. In all the simulations, the iteration tolerance error was 1E-4, and the maximum iteration number was 100 for FOUCSS and 40 for LPISS. The tolerance error for the BFGS optimization in LPISS was 1E-6.

IV. Simulation Results

A. Tests for Two Isolated Sources Under Different NSRs

In this simulation, we tested the noise effect on LORETA, FOCUSS and LPISS when applied to localize two isolated sources. Two dipole sources with moments of (1.90, 0.60, 0.40) and (0.40, 2.30, 0.00) were placed at two isolated positions $(-23.00, -51.00, 51.67)$ (mm) and $(-43.00, -41.00, 61.67)$ (mm), respectively. The scalp potentials were obtained by BEM and contaminated with white Gaussian noise of different NSRs. For different NSR cases, LORETA, FOCUSS, and LPISS were taken for source localization. The E_{energy} and $E_{\text{localization}}$ were calculated within a sphere of 25 mm radius with the center at the corresponding simulated source position. NBI was also estimated within a spherical ROI with 25 mm radius but with the center at the position of the estimated source with the maximum power. For $\text{NSR} = 0\%, 5\%, 10\%, 15\%$, and 20%, the values of λ in LPISS were 0.09, 0.17, 0.34, 0.51, and 0.68, respectively. The localization results under $\text{NSR} = 0.15$ were shown on the MRI slices in Fig. 1 and the corresponding indexes in all noise cases were shown in Fig. 2.

As shown in Figs. 1 and 2, among these three localization algorithms, the estimated sources areas with LORETA were mostly blurring, which usually were the large clouds activated regions on the MRI slices. The $E_{\text{localization}}, E_{\text{energy}}$ and NBI of LORETA were relatively large compared with the other two methods. While in all simulated cases, LORETA could establish a relatively strong source at the corresponding simulated source position like that in the 0.15 noise case shown in Fig. 1, where there was overlapping between the blue cross line and the colorful rectangle area on MRI slices. When $\text{NSR} < 0.10$, the $E_{\text{localization}}$ and NBI of FOCUSS were small, which meant that the localization ability of FOCUSS under low NSR was good for isolated sparse sources. But for the stronger noise cases with $\text{NSR} > 0.10$, FOCUSS was not stable with a remarkable increase of $E_{\text{localization}}$ and E_{energy}. As shown by the localization result of FOCUSS for $\text{NSR} = 0.15$ in Fig. 1, no strong sources were estimated at the corresponding simulated source positions while localized in some other areas close to the due positions instead, and FOCUSS localized some fake weak sources in other areas relatively far away from the simulated sources at the same time. In all the cases, the $E_{\text{localization}}$ of LPISS were nearly 0, except for the case with $\text{NSR} = 0.15$ of the second source, which was localized at a neighboring grid node with $E_{\text{localization}} = 10$ mm. Comparing the localization results of LPISS and FOCUSS under $\text{NSR} = 0.15$ shown in Fig. 1, the source configuration localized by LPISS was much clearer and of fewer fake sources than that localized by FOCUSS. Furthermore, the E_{energy} and NBIs of LPISS were relatively small and changed smoothly. Thus, the calculated three indexes showed that LPISS was relatively stable over different noise levels.

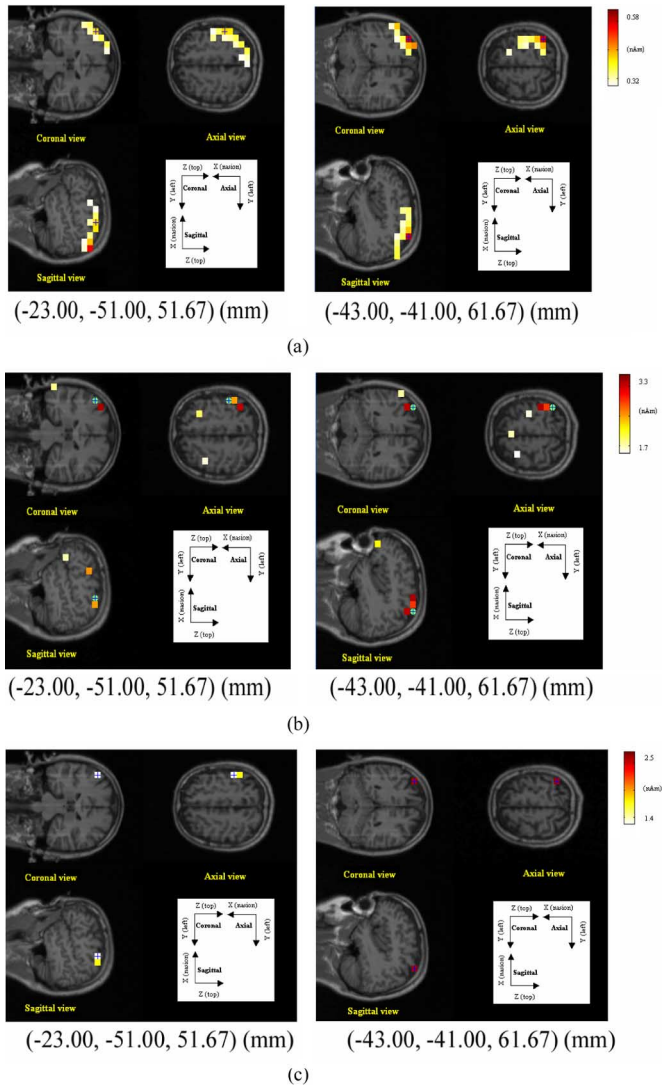

Fig. 1. Localization results of LORETA, FOCUSS and LPISS on MRI slices for two isolated sources under noise of $\text{NSR} = 0.15$. (a) LORETA localized sources; (b) FOCUSS localized sources; (c) LPISS localized sources. Colorful rectangle area is the estimated source location; the blue cross line within the colorful rectangle area indicates the overlapping area of the simulated source and the estimated source; the blue cross line within green circle indicates those simulated source locations that are not overlapped with the positions of the estimated sources.

B. Localization of Deep and Superficial Sources Simultaneously

In this simulation, three dipole sources with moments of (6.00, 2.70, 1.90), $(-8.00, 3.00, 1.00)$ and (5.80, 1.00, 2.00) were placed at three isolated positions $(-83.00, 19.00, 31.67)$

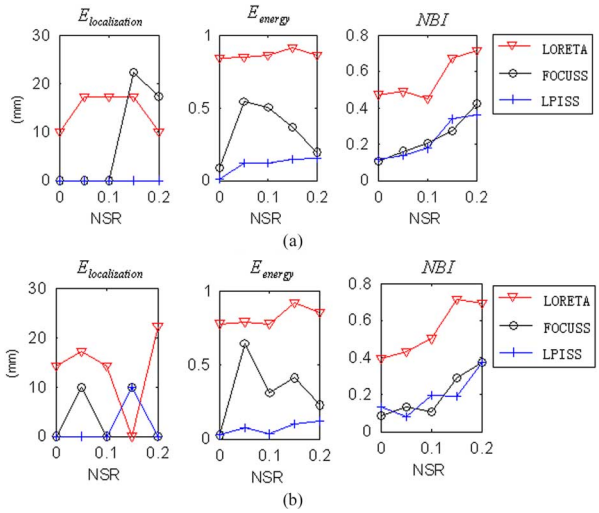

Fig. 2. Localization indexes at different noise NSRs. (a) Source 1; (b) Source 2.

(mm), $(-23.00,\ 29.00,\ -8.33)$ (mm) and $(-63.00,\ 39.00,\ -48.33)$ (mm), among which the first and the third were two superficial sources and the second one was a deep source. The scalp potentials were generated by BEM and contaminated with white Gaussian noise of $\mathrm{NSR} = 0.15$. LORETA, FOCUSS and LPISS were used to localize the sources, and the three indexes, $E_{\mathrm{localization}}, E_{\mathrm{energy}}$, and NBI, were calculated as those in Section IV.A. The value of λ in LPISS was 0.63. The results were shown in Fig. 3 and Table I.

All of the three methods localized the two superficial sources with relatively small distance errors $(E_{\mathrm{localization}})$ and among them, the results of FOCUSS and LPISS were more sparse with relatively smaller NBIs and fewer dipoles. But for the deep source 2, no activation at the true position was found by LORETA and FOCUSS, whereas, with LPISS, the deep source was localized with no distance error and a small NBI. In this case, LPISS and FOCUSS were both initialized with LORETA solution, in which no source with strong power at the deep source position was estimated, but LPISS could still modify the initial distribution and converge to the deep source while FOCUSS failed. This difference between FOCUSS and LPISS was caused by the different methods to evaluate q during the iterations, one was in essence based on the MN solution, the other was based on the l_1 norm sparse solution, and the performance of l_1 norm solution was usually superior to the MN solution in EEG inverse problem [1], [30].

C. Localization of Focally Extended Source

The above simulations were all for the configurations consisting of far isolated sources, here shown were the localization results for a focally extended source. 17 dipole sources were placed within a sphere centered at $(-73, -41, 31.667)$ (mm) with radius of 15 mm. Moment component of each dipole was randomly set within range [0, 10]. The test was conducted under $\mathrm{NSR} = 0.15$. The above three indexes for this focally extended source were calculated as follows. The dipole source with the maximum power in the simulated sources was taken as the reference dipole. The distance error, $E_{\mathrm{localization}}$, was the distance

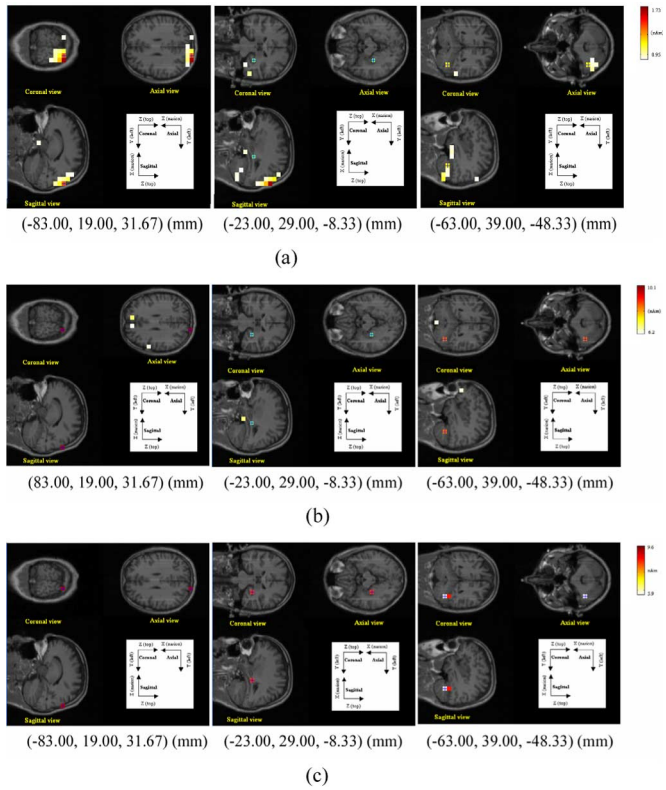

Fig. 3. Localization results of LORETA, FOCUSS and LPISS on MRI slices at the simulated source positions for three isolated sources under noise of NSR=0.15. (a) LORETA localized sources; (b) FOCUSS localized sources; (c) LPISS localized sources. Colorful rectangle area is the estimated source location; the blue cross line within the colorful rectangle area indicates the overlapping area of the simulated source and the estimated source; the blue cross line within green circle indicates those simulated source locations that are not overlapped with the positions of the estimated sources. In LORETA results (a) and FOCUSS results (b), no corresponding sources at the position of simulated deep source 2 were found.

TABLE I
EVALUATION INDEXES FOR THREE SOURCES UNDER NOISE OF $\mathrm{NSR} = 0.15$

	Source 1			Source 2			Source 3		
	LORETA	FOCUSS	LPISS	LORETA	FOCUSS	LPISS	LORETA	FOCUSS	LPISS
E_{energy}	0.8980	0.4419	0.2502	0.9749	0.7566	0.1748	0.9152	0.2192	0.3721
$E_{localization}$ (mm)	10.000	0	0	22.3607	22.3607	0	17.3205	0	10
NBI	0.5784	0.1045	0.1378	0.6311	0.0732	0.1189	0.4794	0.1178	0.2574

between the reference dipole and the dipole with the maximum power in the estimated sources [1]. NBIs were calculated within a 30 mm-sphere centered at the positions of the simulated and estimated dipoles with maximum powers, respectively. And the average power of the extended source, P_{average}, was obtained over all the simulated or estimated sources, respectively. The value of λ in LPISS was 0.95. The localization results on MRI slices near the simulated sources area were shown in Fig. 4 and the indexes were listed in Table II, too.

On the MRI slices, the estimated sources area with LORETA was much broader than actually it was, and those of LPISS and FOCUSS were much more sparse and local than the true case.

Totally 40 relatively strong sources near the simulated area were found with LORETA, and using FOCUSS and LPISS, only

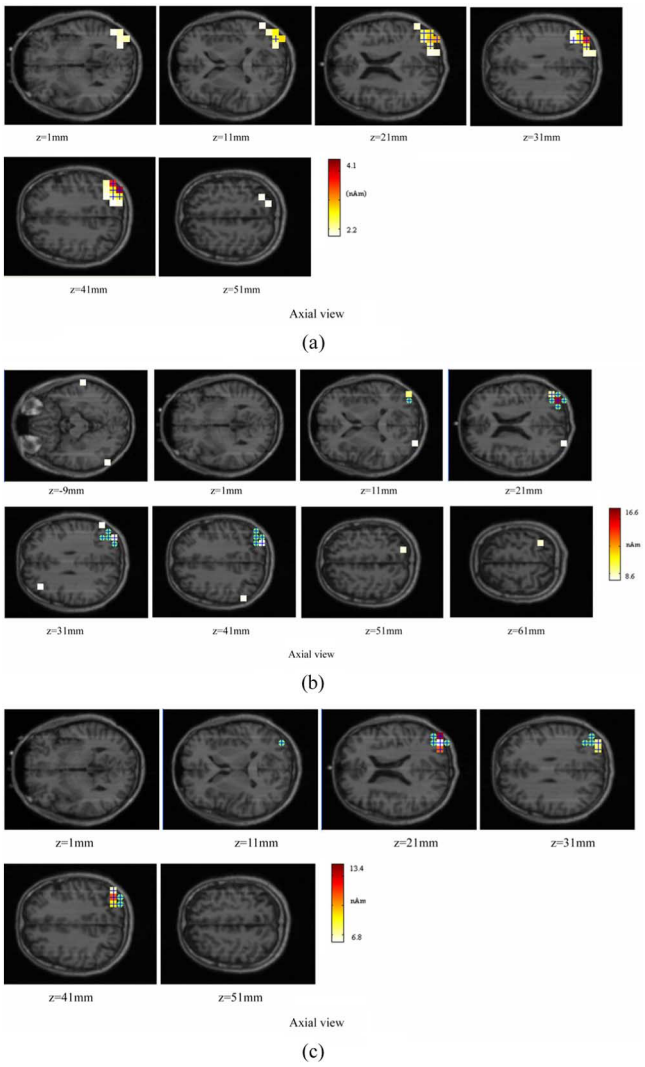

Fig. 4. Localization results of LORETA, FOCUSS, and LPISS on MRI slices near the simulated sources area for a focally extended source under noise of $\mathrm{NSR} = 0.15$. (a) LORETA localized sources; (b) FOCUSS localized sources; (c) LPISS localized sources. Colorful rectangle area is the estimated source location; the blue cross line within the colorful rectangle area indicates the overlapping area of the simulated source and the estimated source; the blue cross line within green circle indicates those simulated source locations that are not overlapped with the positions of the estimated sources.

TABLE II
EVALUATION INDEXES FOR EXTENDED SOURCE UNDER NOISE OF $\mathrm{NSR} = 0.15$

Index	Simulation	LORETA	FOCUSS	LPISS
NBI	0.5088	0.5709	0.2179	0.4550
$E_{localization}\ (mm)$	0.0000	17.3205	10.0000	14.1421
$P_{average}$	64.3200	12.1725	135.4317	78.7437

14 and 8 sources were localized, respectively. The NBIs of FOCUSS and LPISS were 0.2179 and 0.4550, which were both smaller than the actual NBI (0.5088) of the original extended source, and contrary was that (0.5709) of LORETA. The fact means that, with the emphasis on the sparsity of the extended source, FOCUSS and LPISS may converge to a sparser solution with fewer dipoles, and due to the smoothing effect of the spatial Laplacian operator, LORETA will enlarge and blur the simulated source area. Certainly, the ideal result is that all the simulated extended source could be recovered correctly, but it is rather difficult for EEG inverse problem, and generally if most of the estimated sources are located near or within the simulated area and the difference of NBI between the simulated extended source and the estimated extended source is not too large, the localization could be thought to be successful for the extended source [29]. As shown by the estimated source locations on MRI slices and the indexes in Table II, FOCUSS had the smallest $E_{\mathrm{localization}}$ (10 mm), but with some estimated sources out of the assumed area; the $E_{\mathrm{localization}}$ of LORETA and LPISS were 17.3205 mm and 14.1421 mm, and the sources estimated by LORETA and LPISS were basically distributed within the simulated area. Thus, we may say that these three methods all localized this simulated activated area successfully. Each of them established a corresponding equivalent source distribution for the simulated extended source, and the differences among the estimated results were that the result of LORETA was a blurring and enlarged area, and the other two were two sparse and focal areas. By comparison of P_{average}, the P_{average} (78.7437) of LPISS was much closer to the actual P_{average} (64.3200) than those of LORETA (12.1725) and FOCUSS (135.6725), thus, LPISS recovered the source power more originally than the other two methods did. This simulation also showed that different localization methods may result in some different equivalent source distributions and the difference should be taken into account in explanation of the results for an EEG inverse problem, especially for the real EEG data [29].

D. Statistical Features of the Localization Methods

Generally, the detailed performance of a localization algorithm depends on the head model and source configuration, etc [1], [30]. In this section, the performances of these three algorithms were evaluated by a way similar to the Mont-Carlo simulation. In literature [5], by placing one dipole source on each grid node of the solution space, $E_{\mathrm{localization}}$ and E_{energy} between the simulated source and the estimated source with maximum power were calculated for each grid node, and then the mean and standard deviation (SD) of $E_{\mathrm{localization}}$ and E_{energy} were calculated, respectively. In this paper, for reducing the computation load, we tested the localization performance on 100 randomly selected positions, and for each of the 100 positions, a dipole with moment randomly varied within $[-10, 10]$ was put on it. For each case, the simulated scalp data was mixed with noise at $\mathrm{NSR} = 10\%$. $E_{\mathrm{localization}}$ and E_{energy} were calculated between the simulated source and the estimated source with maximum power, and NBI was calculated at the position of the estimated source with maximum power. The mean and SD of the three evaluation indexes for the 100 cases were shown in Fig. 5.

V. REAL DATA TEST

A. IOR Experiment

We adopted the modified classical experiment paradigm of inhibition of return (IOR), designed by Posner [22], to acquire the ERP recordings. The visual stimuli were generated by a personal computer and the adopted behavioral task was illustrated

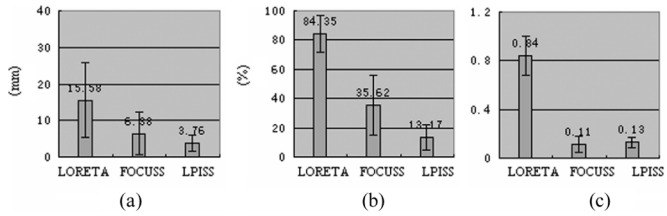

Fig. 5. Statistical features of the three localization methods. (a) Mean and SD of $E_{\text{localization}}$; (b) Mean and SD of E_{energy}; (c) Mean and SD of NBI.

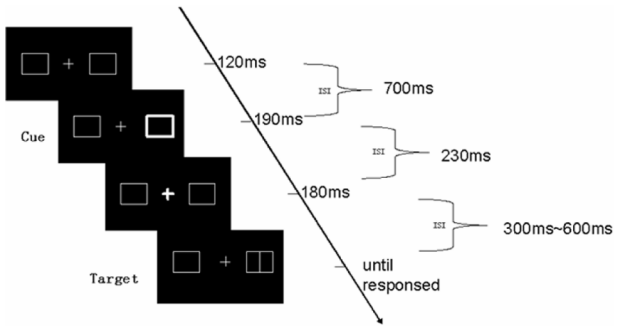

Fig. 6. An example of the stimulus display sequences used in the IOR experiment. The cue is a brightening of an unfilled box centered around one of the two peripheral target locations; the target is a vertical line in the box.

in Fig. 6. The background was dark and the center fixation point was a cross with 0.5° visual angle. Each of the two rectangle outline boxes was of size $1.5° \times 1.0°$ visual angle and was horizontally located with 5° visual angle from the fixation. Brightening of one of the boxes served as the "cue", and the target, either a short vertical line (0.75° visual angle) or a long vertical line (1.0° visual angle), was presented within either of the two boxes with equal probability. The experiments were carried out in a dark room with subjects seated 50 cm in front of monitor and instructed to fix on the fixation cross.

The initial display, consisting of two boxes located in the right and left of the central fixation, was presented for 120 ms. After a 700 ms inter-trial interval (ISI), one of the boxes was then cued by outlining the perimeter of the box for 190 ms. After a delay of 230 ms, the central fixation cross was brightened for 180 ms. And following a randomly variant delay from 300 ms to 600 ms after the central cued fixation cross disappeared, the target was presented until the subject responded. Both the cue and the target were presented with equal probability within one of the boxes randomly. Subjects were instructed to press the button as quickly as possible whenever they saw the target, key "1" for the short line and key "4" for the long line. 15 subjects performed the same practice consisting of 10 experimental blocks, 80 trials in each block.

EEG was recorded with the 128-channel EGI system at sampling rate of 250 Hz, and vertex (Cz) was taken as the reference. Epochs contaminated with excessive eye movements, blinks, muscle artifacts, or amplifier blocking were manually removed prior to averaging, and recordings of 13 in 15 subjects were valid for further processing. According to the different locations of the presented cue and target (RR: right cue-location and right target-location; RL: right cue-location and left target-location;

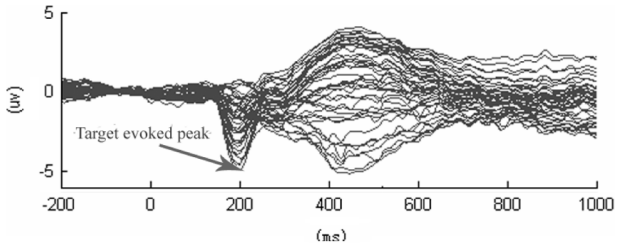

Fig. 7. ERP of the case with cue at right and target at right (RR).

LL: Left cue-location and left target-location; LR: Left cue-location and right target-location), the epochs in recordings for each subject were classified into four kinds of ERPs, i.e., RR, RL, LL, and LR. Each epoch, 1.2 s long, started 200 ms before the onset of the target and continued for 1000 ms after the onset of the target. Epochs in the 13 valid subjects were grandly averaged to get 4 kinds of ERPs according to the four location combinations of cue and target. In this paper, reported was the result of RR.

B. Results and Discussion

Behavior experiments show that for longer stimulus-onset-asynchronies (SOAs, usually longer than 250 ms), subjects are slower to respond to targets presented at the cued location (valid-cue) than to targets presented at uncued locations (invalid-cue), and it is the phenomenon of inhibition of return (IOR) discovered by Poser [23] and many brain function areas are suggested to be involved in the IOR process [24]–[28].

As shown in Fig. 7, in our IOR experiment, the IOR related ERP elicited by the target shows a significant peak at 200 ms after the onset of the target, and the following analysis is focused on this component. According to the usual ERP case, the NSR is supposed to be 0.15.

The localized activations by LORETA, FOCUSS, and LPISS were shown in Figs. 8, 9, and 10, respectively. The value of λ in LPISS was assumed to be 0.63.

Since the phenomenon of IOR was discovered by Posner in 1984, the neural and psychological mechanisms of IOR have been a popular subject of much controversy and debate. With empirical supports, some researchers suggested that IOR is a bias of attention. Others, however, have proposed that IOR is the activation of the oculomotor system. Recently, some evidences suggested that both attention and motor systems might be involved in the generation of IOR [24].

As for the neurophysiologic mechanism, evidences have been found that the generation of IOR is related to the superior colliculus [23]–[25], which is involved in both attention and oculomotor process [24], [26]. By the single-pulse transcranial magnetic stimulation (TMS) and fMRI, the frontal eye fields (FEF) were found to play a crucial role in the generation of IOR [26], [27].

Activations in the right cerebellum were found to be obviously elicited when covert spatial-attention shifts were compared to eye movements [27], [28]. As the IOR experiment mode involves spatial-attention orienting process [22] and previous researches showed that right cerebellum was often activated during the attention shift process in human brain.

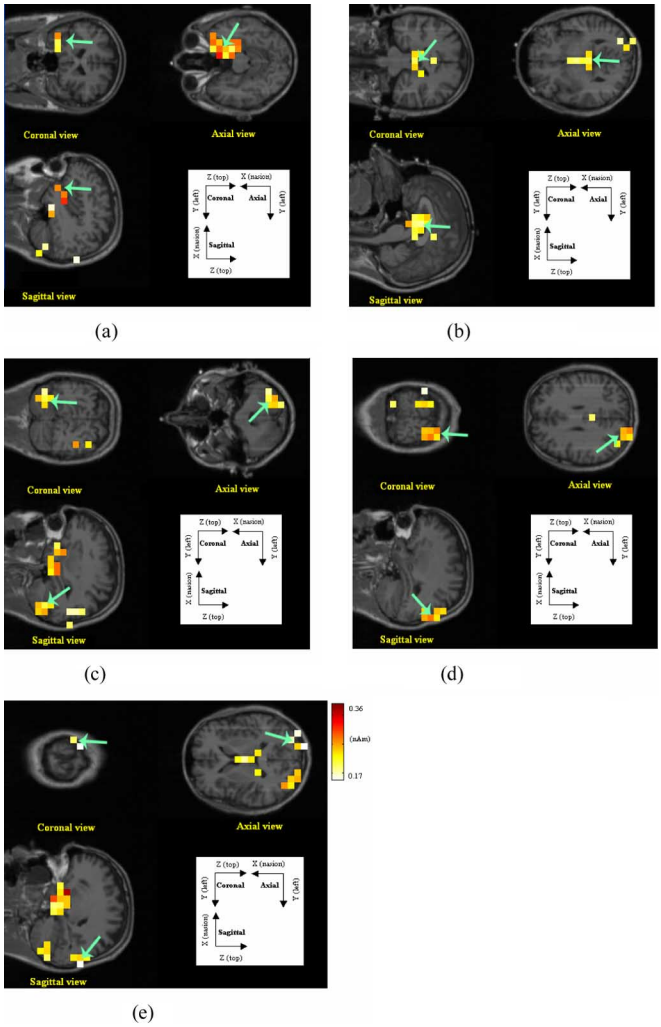

Fig. 8. LORETA. (a) right frontal eye fields; (b) thalamus; (c) right cerebellum; (d) letf occipital; (e) right occipital.

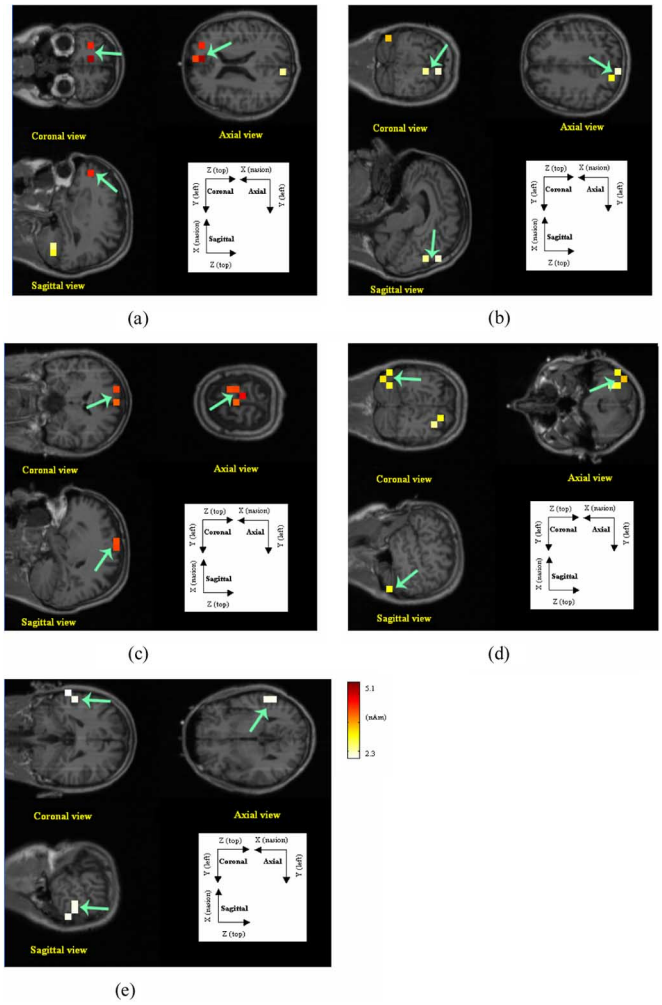

Fig. 9. FOCUSS. (a) right frontal eye fields; (b) left occipital; (c) paretial; (d) right cerebellum; (e) right lateral occipital-paretial.

As shown in above figures, the activations in the right frontal eye fields and the right cerebellum were all detected by these three methods. Furthermore all these three methods localized activations in the left occipital. Because the RR data was generated with cue and target both presented at right, some related areas in the left occipital might be invoked.

Both LORETA and LPISS detected relatively strong activations in the thalamus, while FOCUSS localized a relatively superficial activations in the paterial. It may be the activations in the thalamus bias toward the surface just as the localization of the deep source in Section IV.C. Similar to the simulations, activations detected by LORETA were of large area and the activations localized by FOCUSS and LPISS were relatively sparse and local.

VI. Discussions and Conclusion

The above simulations show that LPISS has good ability to localize the isolated sparse sources, even for the deep source. Among LPISS, FOCUSS and LORETA, LPISS shows the best performance as evaluated by the three indexes for isolated sources. For the tested source configurations, LPISS produced reasonable sparse solutions, FOCUSS somewhat depended on the noise level and source configurations, and LORETA usually generated blurred results. The improvement of LPISS compared with FOCUSS is that the $l_p(p \leq 1)$ norm is integrated into the iterative procedure of FOCUSS, whereas, the original FOCUSS procedure in essence uses the minimum norm solution, and the $l_p(p \leq 1)$ norm solution is usually superior to the MN solution in EEG inverse problem, thus, both the $l_p(p \leq 1)$ norm and the iterative weight force the solution to converge to a sparse and reasonable solution. And naturally, in the simulation test for the focally extended source, a more focal and sparse source area than actually the situation was is estimated with LPISS. And this simulation shows that LPISS was not very qualitified for extended source because of its emphasis on the sparsity of the resulted sources configuration.

In Section IV.D, we systematically tested the localization performance of LORETA, FOCUSS and LPISS using a Mont-Carlo like simulation. As shown in Fig. 5, LPISS showed a much better localization performance than the other two methods. In this Mont-Carlo like simulation, the source configuration is simple with only one dipole source for each case, and the localization of such simple source configuration is usually easier than localization of a complex source configuration. Certainly, when localizing for other complex source configuration,

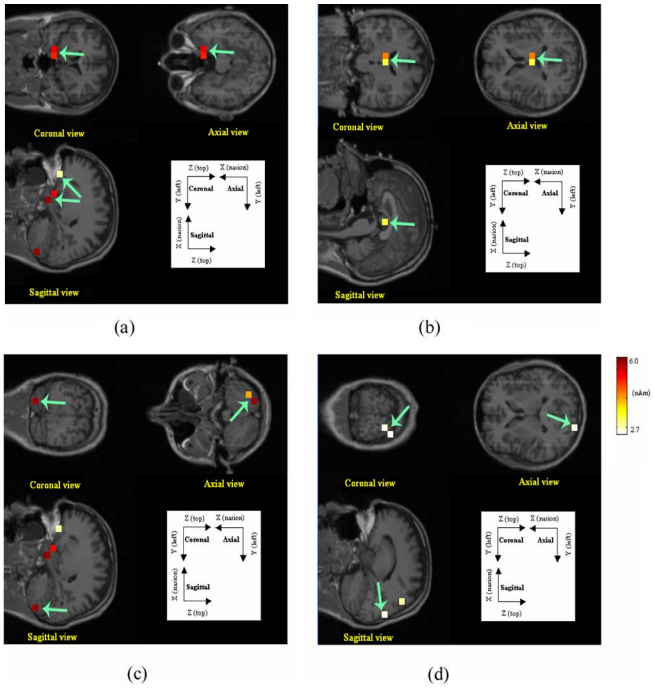

Fig. 10. LPISS. (a) right frontal eye fields; (b) thalamus; (c) right cerebellum; (d) left occipital.

the performance of a method would accordingly be somewhat lowered as shown by the above simulated situations.

For the real IOR data, using LPISS, the activations were localized in the right thalamus, the right frontal eye fields, the right cerebellum and the left occipital, consistent with the reports in some previous studies [24], [27]. Among the results of LORETA, FOCUSS and LPISS, the activations localized by LORETA were more extended, and those of FOCUSS and LPISS were relatively focal and sparse. Furthermore, there are also some differences among the results of these three methods, just like the localization results of the simulated extended source in Section IV. These facts mean that, for the EEG inverse problem, different localization methods may result in different equivalent sources, and for different actual problems, the difference among different localization methods should be taken into account [29].

In this paper, we implicitly assumed the residual error is of Gaussian distribution, thus, we designed the cost function as a combination of a l_2 norm of the residual errors and a l_1 norm of the regularization term in solving the $l_p(p \leq 1)$ norm constrained problem for a sparse solution of q, and in this way, we have part of our cost function similar to the popular EEG inverse algorithms, including FOCUSS and LORETA, thus, gave us hint to evaluate LPISS by comparing it with LORETA and FOCUSS. However, in general, we may also apply $l_p(p \leq 1)$ norm for both the residual error and the regularization terms in (10), and it may result in a novel solution different from the current EEG inverse solutions. Apparently, it is a valuable project for the future.

In this paper, the classical $1/80$ was adopted as the conductivity ratio between the skull and the brain [31]. However, in recent years, some different values varying from $1/50$ to $1/15$ was suggested for the skull-brain conductivities ratio [32], [33]. And the different skull conductivity may have some effect on the performance of a source localization algorithm. And in order to reduce the effect of the conductivity on the evaluation of different methods, we used the same skull conductivity for all methods, thus, the comparison is fair and can reveal the difference among different localization methods. The effect of different conductivities on the localization methods needs to be further studied.

In literature [9], it has been proved that FOCUSS is absolutely convergent with at least a quadratic rate of convergence. LPISS is based on the iterative procedure same as that of FOCUSS and the difference between them is only that the sparse and power concentrated solution of the intermediate auxiliary variable q in the iteration is estimated directly, instead of using the minimum norm solution estimated with the pseudo-inverse in FOCUSS. In essence, this substitution will not affect the convergence of the iterative procedure. Compared with FOCUSS, there is no simple solution for the $l_p(p \leq 1)$ norm constrained cost function in (10), LPISS uses an optimization programming to solve the $l_p(p \leq 1)$ norm constrained problem, and it needs much more computation than the solving based on SVD as that in FOCUSS. In this paper, the algorithm was implemented on a normal PC (1.7 GHz, 256 M RAM) under the Matlab 6.5 environment. When localized on the realistic head model, it needs nearly 10 hours. However, along with the rapid progress of the computer science, we believe such a computation will not be a crucial problem in the near future.

REFERENCES

[1] C. M. Michel and M. Murray, "EEG source imaging," *Clin. Neurophysiol.*, vol. 115, pp. 2195–2222, 1997.
[2] R. D. Pascual-Marqui, C. M. Michel, and D. Lehmann, "Low resolution electromagnetic tomography: A new method for localizing electrical activity in the brain," *Int. J. Psychophysiol.*, vol. 18, pp. 49–65, 1994.
[3] J. Z. Wang, S. J. Williamson, and L. Kaufman, "Magnetic source images determined by a lead-field analysis: The unique minimum-norm least-squares estimation," *IEEE Trans. Biomed. Eng.*, vol. 39, pp. 665–675, 1992.
[4] C. Silva, J. C. Maltez, and E. Trindade, "Evaluation of L_1 and L_2 minimum norm performances on EEG localizations," *Clin. Neurophysiol.*, vol. 115, pp. 1657–1668, 2004.
[5] H. S. Liu and X. R. Gao, "A recursive algorithm for the three-dimensional imaging of brain electric activity: Shrinking LORETA-FOCUSS," *IEEE Trans. Biomed. Eng.*, vol. 51, no. 10, pp. 1794–1802, Oct. 2004.
[6] D. Yao and B. He, "A self-coherence enhancement algorithm and its application to enhancing 3D source estimation from EEGs," *Ann. Biomed. Eng.*, vol. 29, no. 11, pp. 1019–1027, 2001.
[7] M. Scherg and D. Von Cramon, "Evoked dipole source potentials of the human auditory cortex," *Electroencephalogr Clin. Neurophysiol.*, vol. 65, pp. 344–360, 1986.
[8] D. Yao, "The equivalent source technique and cortical imaging," *Electroencephalogr. Clin. Neurophysiol.*, vol. 98, pp. 478–483, 1996.
[9] I. F. Gorodnitsky and B. D. Rao, "Sparse signal reconstruction from limited data using FOCUSS: A re-weighted minimum norm algorithm," *IEEE Trans. Signal Process.*, vol. 45, no. 3, pp. 600–616, Mar. 1997.
[10] B. D. Rao, "Analysis and extensions of the FOCUSS algorithm," in *Proc. Asilomar*, 1996, vol. 2, pp. 1218–1223.
[11] D. Yao and B. He, "The Laplacian weighted minimum norm estimated of three-dimensional equivalent charge distribution in the brain," in *Proc. IEEE/EMBS Conf.*, 1998, vol. 20, pp. 2108–2111.
[12] B. He, D. Yao, J. Lian, and D. Wu, "An equivalent current source model and Laplacian weighted minimum norm current estimates of brain electrical activity," *IEEE Trans. Biomed. Eng.*, vol. 4, pp. 277–288, Apr. 2002.

[13] J. F. Murray and K. Kreutz-Delgado, "An improved focuss-based learning algorithm for solving sparse linear inverse problems," in *Rec. 35th Asilomar Conf. Signals, Systems and Computers,* , 2001, vol. 1, pp. 4–7.
[14] P. Bofill and M. Zibulevsky, "Underdetermined blind source separation using sparse representations," *Signal Process.*, vol. 81, pp. 2353–2362, 2001.
[15] M. Zibulevsky and Y. Zeevi, "Extraction of a source from multichannel data using sparse decomposition," *Neurocomputing*, vol. 49, pp. 163–173, 2002.
[16] A. Ossadtchi and S. Kadambe, "Over-complete blind source separation by applying sparse decomposition and information theoretic based probabilistic approach," in *Proc. IEEE Int. Conf. Acoustics, Speech, and Signal Processing*, 2001, vol. 5, pp. 2801–2804.
[17] S. Chen, D. L. Donoho, and M. Saunders, "Atomic decomposition by basis pursuit," in *SIAM J. Sci. Comp.*, 1999, vol. 20, no. 1, pp. 33–61.
[18] A. N. Tikhonov and V. Y. Arsenin, *Solutions of Ill-Posed Problems*. New York: Wiley, 1977, (Trans. from Russian).
[19] D. H. Li and M. Fukushima, "A modified BFGS method and its global convergence in nonconvex minimization," *J. Comp. Appl. Math.*, vol. 129, pp. 15–35, 2001.
[20] M. Fuchs and R. Drenckhahn, "An improved boundary element method for realistic volume-conductor modeling," *IEEE Trans. Biomed. Eng.*, vol. 45, no. 8, pp. 980–997, Aug. 1998.
[21] Net Station Viewer Technical Manual Electrical Geodesics, Inc.. Eugene, OR, pp. 153–166, 2003.
[22] M. I. Posner and Y. Cohen, "Components of visual orienting," in *Attention and Performance*, H. Bouma and D. Bouwhhuis, Eds. Hillsdale, NJ: Erlbaum, 1984, pp. 531–556.
[23] M. I. Posner, R. D. Rafal, L. S. Choate, and J. Vaughan, "Inhibition of return: Neural basis and function," *Cogn. Neuropsychol.*, vol. 2, pp. 211–228, 1985.
[24] R. M. Klein, "Inhibition of return," *Trends Cogn. Neurosci.*, vol. 4, pp. 138–147, 2000.
[25] A. Sapir, N. Soroker, A. Berger, and A. Henik, "Inhibition of return in spatial attention: Direct evidence for collicular generation," *Nature Neurosci.*, vol. 2, pp. 1053–1054, 1999.
[26] T. Ro, A. Farne, and E. Chang, "Inhibition of return and the human frontal eye fields," *Exper. Brain Res.*, vol. 150, pp. 290–296, 2003.
[27] J. Lepsien and S. Pollmann, "Covert reorienting and inhibition of return: An event-related fMRI study," *J. Cogn. Neurosci.*, vol. 14, pp. 127–144, 2002.
[28] M. Corbetta, E. Akbudak, T. E. Conturo, A. Z. Snyder, J. M. Ollinger, H. A. Drury, M. R. Lineweber, and S. E. Petersen, "A common network of functional areas for attention and eye movements," *Neuron*, vol. 21, pp. 761–773, 2002.
[29] C. Grova, J. Daunizeau, J.-M. Lina, C. G. Be'nar, H. Benali, and J. Gotman, "Evaluation of EEG localization methods using realistic simulations of interictal spikes," *Neuroimage*, vol. 29, pp. 734–754, 2006.
[30] R. D. Pascual-Marqui, "Review of methods for solving the EEG inverse problem," *Int. J. Bioelectromagn.*, vol. 1, pp. 75–86, 1999.
[31] S. Rush and D. A. Driscoll, "EEG electrode sensitivity-an application of reciprocity," *IEEE Trans. Biomed. Eng.*, vol. 16, no. 1, pp. 15–22, Jan. 1969.
[32] Y. Lai, W. van Drongelen, L. Ding, K. E. Hecox, V. L. Towle, D. M. Frim, and B. He, "*In vivo* human skull conductivity estimation from simultaneous extra- and intra-cranial electrical potential recordings," *Clin. Neurophysiol.*, vol. 116, no. 2, pp. 456–465, 2005.
[33] S. Goncalves, J. C. de Munck, J.P.A. Verbunt, F. Bijma, R. M. Heethaar, and F. H. Lopes da Silva, "*In vivo* measurement of the brain and skull resistivities using an EIT-based method and realistic models for the head," *IEEE Trans. Biomed. Eng.*, vol. 50, no. 6, pp. 754–767, Jun. 2003.

Peng Xu received the Ph.D. degree in biomedical engineering from the University of Electronic Science and Technology of China (UESTC), Chengdu, China, in 2006.

His research interest includes biomedical signal processing and medical image analysis.

Yin Tian is working towards the Ph.D. degree in the University of Electronic Science and Technology of China, Chengdu, China.

Her research interests include selective attention, cognitive brain research of inhibition of return.

Huafu Chen received the Ph.D. degree in biomedical engineering from the University of Electronic Science and Technology of China (UESTC), Chengdu, China, in 2004.

He is the author or coauthor of more than 50 scientific papers. He is currently a Professor in the School of Life Science and Technology at UESTC. His major research interests include independent component analysis, functional magnetic resonance imaging, and signal and image processing.

Dezhong Yao received the Ph.D. degree in applied geophysics from Chengdu University of Technology, Chengdu, China, in 1991, and completed the postdoctoral fellowship in electromagnetic field at the University of Electronic Science and Technology of China (UESTC), Chengdu, China, in 1993.

He has been a faculty member since 1993; a Professor since 1995 and, since 2001, Dean of the School of Life Science and Technology at UESTC. He was a Visiting Scholar at University of Illinois at Chicago from September 1997 to August 1998, and a Visiting Professor at McMaster University, Hamilton, ON, Canada, from November 2000 to May 2001, and at Aalborg University, Aalborg, Denmark, from November 2003 to February 2004. He is the author or coauthor of more 80 papers and five books. His current interests include EEG, fMRI, and their applications in cognitive science and neurological problems.